(5) C. Domb, *J. Chem. Phys.*, **38**, 2957 (1963).
(6) F. T. Hioe, Ph.D. Thesis, University of London, London, England, 1967.
(7) (a) P. G. Watson, *Physica*, **75**, 627 (1974); (b) P. G. Watson, *J. Phys. C:*, **3**, L23 (1970).
(8) F. T. Wall, S. Windwer, and P. J. Gans, *J. Chem. Phys.*, **38**, 2228 (1963).
(9) J. Mazur and F. L. McCrackin, *J. Chem. Phys.*, **49**, 648 (1968).
(10) S. Windwer, *J. Chem. Phys.*, **43**, 115 (1965).
(11) (a) R. J. Fleming, *J. Phys. A:*, **1**, 404 (1968); (b) N. C. Smith and R. J. Fleming, *ibid.*, **8**, 929, 938 (1974).
(12) E. Loftus and P. J. Gans, *J. Chem. Phys.*, **49**, 3828 (1968).
(13) W. Bruns, *Makromol. Chem.*, **134**, 193 (1970); **124**, 91 (1969).
(14) M. Lax and S. Windwer, *J. Chem. Phys.*, **55**, 4167 (1971).
(15) Z. Alexandrowicz and Y. Accad, *Macromolecule*, **6**, 251 (1973).
(16) A. K. Kron and O. B. Ptitsyn, *Vysokomol. Soedin.*, **6(5)**, 862 (1964).
(17) C. Domb and G. S. Joyce, *J. Phys. C:*, **5**, 956 (1972).
(18) C. Domb and A. J. Barrett, *Polymer*, in press.
(19) C. Domb, A. J. Barrett, and M. Lax, *J. Phys. A:*, **6**, 282 (1973).
(20) A. J. Barrett, Thesis, University of London, 1975.
(21) M. F. Sykes, *J. Chem. Phys.*, **39**, 410 (1963).
(22) A. J. Barrett, *J. Phys. A:*, **9**, L33 (1976).
(23) This universal expression for α^2 should be strictly correct in the limit $\omega \to 0$, $N \to \infty$, η finite.

Monte Carlo Calculations on Polypeptide Chains. 10. A Study of the Kinetics of the Helix–Coil Transition

Darrow E. Neves and Roy A. Scott III*

Department of Biochemistry, The Ohio State University, Columbus, Ohio 43210.
Received June 23, 1976

ABSTRACT: A stochastic model of the kinetics of the helix–coil transition based on the equilibrium statistical mechanical theory of Lifson and Roig is presented. A Monte Carlo simulation of the kinetics based on the stochastic model was used to study the kinetics of the helix–coil transition. Kinetics simulations were conducted from several initial values of the fractional hydrogen bonding parameter θ to each equilibrium value of θ. A spectrum of relaxation times and characteristic weighting constants is reported for each kinetics simulation. The chain lengths used in this study were 15, 34, and 85 residues. It was found that at each chain length the relaxation times depend only on the equilibrium value of θ while the characteristic weighting constants depend on both the initial and equilibrium values of θ. The mean relaxation time was calculated for several relaxations at chain lengths 15, 34, and 85. It was found that the mean relaxation time does not reflect the correct order of magnitude of the slowest relaxation process. In addition, it was found that pure random coil species do not survive long enough to be measured by nmr spectroscopy and therefore values of $\tau \geq 10^{-1}$ s do not reflect a relaxation time of the helix–coil transition.

I. Introduction

Rapid advancements have been made in treating macromolecular chain conformations by equilibrium statistical mechanics.[1-3] This progress has been due in large measure to the adoption of Volkenstein's rotational isomeric state approximation[1] which allowed the mathematical formalism of the Ising lattice model to be applied to this important area of research. Recent improvement in the mathematical formalism, developed by Flory and his co-workers[3] using improved matrix methods, has resulted in a very elegant and practical mathematical formulation which has found widespread use. These methods have been applied prolifically to biopolymers, especially to the helix–coil transition in polypeptides and nucleic acids.[4]

Unlike the situation for the equilibrium theory, the rate theory of macromolecular conformational changes is not well developed. There are several theories of the kinetics of the helix–coil transition in polypeptides, however, they are either limited to treatment of only the initial rate[5-7] or to perturbations from equilibrium so large that the reverse reaction is negligible.[8] The initial rate treatment has been widely used to interpret experimental kinetics data obtained using such physical techniques as temperature jump, ultrasonic absorption, and dielectric relaxation. Using these techniques, relaxation times of the order of magnitude of 10^{-5}–10^{-8} s have been reported. Nuclear magnetic resonance spectroscopy has been used to study the helix–coil transition under equilibrium conditions.[9,10] Lifetimes of peaks in the NMR spectra, which have been attributed to the helix and random coil, are reported to be greater than 10^{-1} s.[9] Several workers[11,12] have investigated this apparent contradiction in relaxation times and have attempted to show that the slow relaxation time is due to polydispersity. For example, Bradbury et al.[22] compared fractionated and unfractionated samples using NMR and ORD. These authors concluded that it was highly likely that the α-CH doublet appearing in NMR spectra is due to polydisperse samples. However, considerable controversy remains concerning the nature of the slow relaxation time obtained using NMR spectroscopy.

In this paper we present a stochastic model of the kinetics of the helix–coil transition based on the equilibrium statistical mechanical theory of Lifson and Roig.[13] Using this model, we introduce a Monte Carlo method of simulating the relaxation from an initial value of the fractional helix content θ to an equilibrium value of θ. The equilibrium sample generated in this manner was used previously to study the effect of excluded volume on the helix–coil transition.[14] The chain lengths studied in this paper are 15, 34, and 85 monomers in length. A spectrum of normal modes of relaxation with characteristic amplitudes is reported for all three chain lengths using several initial and equilibrium values of θ. The mean relaxation time will be calculated for several relaxations in order to relate the Monte Carlo results to experimental data. In addition, it will be shown that a slow relaxation time of 10^{-1} s is inconsistent with the survival time of the pure random coil.

II. Models and Methods

In the theory of the helix–coil transition, Lifson and Roig[13] defined the statistical weight parameters u, v, and w as configuration integrals over φ–ψ space, u over the values of φ and ψ in the coil region of a single unit, v over the helical region of such a unit, and w over three consecutive helical units. A polypeptide chain in a given conformation can then be divided into alternating sequences of coil states with statistical weight

u^{n_c} and helical states with statistical weight $v^2w^{n_h-2}$ where n_c and n_h are the number, respectively of coil and helical φ–ψ pairs in a sequence. Isolated helical states, i.e., a helical state which does not have a neighbor in the helical state, have statistical weight v. Since only the relative values of these statistical weights is of physical significance, the usual procedure is to set $u = 1$ and treat v and w as the adjustable parameters.

The stochastic model[15] is introduced by defining three transition probability parameters p, q, and α. q is the probability per unit time that a residue in the coil state will make a transition to the α-helical state. Since the coil state represents all φ–ψ states except the α-helical state, q is an average probability of transition from the coil state to the α-helical state. We assume that the probability of all c → h transitions is q, independent of the state of neighboring residues, i.e., a c state must pass across some energy barrier which for a c state is unaffected by the states of the other units in the chain. After passing across the energy barrier the new h state gains increased stability if it is added to a sequence of at least two or more h states. p is the probability per unit time that an h state, which is not part of a hydrogen-bonded α-helical sequence, will make a transition to the c state. αp is the probability per unit time that one hydrogen bond will be broken, i.e., an h state at the end of an α-helical sequence will make a transition to the coil state. For a sequence of three or more residues in the helical state, the probability that they all make the transition to the coil state is $\alpha^{n_h-2}p^{n_h}$ where n_h is the number of residues in the α-helical sequence. Thus α reflects the increased energy required to break an α-helical hydrogen bond.

By mass balance considerations, we relate the statistical weight parameters u, v, and w to the transition probabilities p, q, and α. For example, . . . chhhc . . . ⇄ . . . ccccc . . . yields $v^{-2}w^{-1}u^3 = \alpha p^3 q^{-3}$. Setting $u = 1$, these expressions reduce to eq 1 and 2.

$$q = vp \tag{1}$$

$$\alpha = vw^{-1} \tag{2}$$

Thus, using the Lifson–Roig theory as a basis for the stochastic model requires the introduction of one additional independent adjustable parameter. If we know v and w, we can calculate α directly from eq 2 and we have a relationship between p and q in eq 1. In the equilibrium theory we have the relative statistical weights v and w by setting $u = 1$. Similarly in the stochastic model, we can define relative transition probabilities q and α by setting $p = 1$. We choose p because it is the largest of the three parameters, i.e., represents the fast h → c process. Choosing $p = 1$ introduces a fundamental time unit of duration p^{-1} into this model. This time unit is sufficiently long to permit isolated h states to make the transition to the c state with probability 1. In all the calculations presented in this paper time will be measured in p^{-1} units.

In other models of the kinetics of the helix–coil transition in polypeptides[15-17,25] the growth reaction is written

$$\text{ccchhhccc} \underset{k_b}{\overset{k_f}{\rightleftarrows}} \text{ccchhhhcc} \tag{3}$$

with $w = k_f/k_b$. k_f is the rate constant for adding a single h state to a preexisting α-helical sequence. In our transition probability notation, $k_f = q(1-q)^5(1-\alpha p^3)$ where $(1-q)$ and $(1-\alpha p^3)$ are the probabilities of a coil state and a hydrogen bond, respectively, surviving for a time period of p^{-1}. In eq 3 k_b is the rate constant for removal of an h state from an α-helical sequence. In transition probability notation, $k_b = \alpha p(1-\alpha p^3)(1-q)^5$. The nucleation reaction is written:

$$\text{ccccccccc} \underset{k_b}{\overset{v^2k_f}{\rightleftarrows}} \text{ccchhhccc} \tag{4}$$

with $v^2w = v^2k_f/k_b$ which in our transition probability notation is written $q^3/\alpha p^3$. Thus a clear relationship exists between the rate constants k_f and k_b used in other theoretical formulations and our transition probabilities.

$$w = \frac{k_f}{k_b} = \frac{q(1-q)^5(1-\alpha p^3)}{\alpha p(1-\alpha p^3)(1-q)^5} = \frac{q}{\alpha p} \tag{5}$$

The approach to equilibrium is resolvable into normal modes of relaxation each with a characteristic time constant.[5,15,18] This is expressed in eq 6

$$\theta(t) = \theta_\infty + \sum_{i=1}^{n-1} c_i \exp(-t/\tau_i) \tag{6}$$

where the relaxation times τ_i are known to depend only on the equilibrium value of θ, denoted θ_∞. The c_i's, which are the amplitude of each normal mode, are known to depend on both θ at a time equal to zero, denoted θ_0 and θ_∞. It is usually extremely difficult to determine the c's and τ's in eq 6 from experimental data. As a result, experimentalists have resorted to evaluation of the mean relaxation time τ^* given by eq 7[24]

$$1/\tau^* = \sum_{i=1}^{n-1} c_i/\tau_i = \frac{1}{\theta_0 - \theta_\infty}\left[\frac{d\theta}{dt}\right]_{t=0} \tag{7}$$

It can be seen that $1/\tau^*$ is the time derivative of eq 6, where τ^* is thought to be a measure of the time required by the relaxation process.[19]

Since the analytical solution for our stochastic model is impractical to use to obtain numerical results except for chains of only a few residues,[15] we have adopted a Monte Carlo simulation technique to generate numerical solutions. The procedure is to use a starting sample of $\theta_0 = 1, 0$, or an intermediate value of θ_0 obtained from the end point of a previous kinetic simulation. Using the weighting scheme discussed previously, we determine transition probabilities which are characteristic of the end point we desire. This is analogous to experimental techniques of perturbing a system such as temperature jump, dielectric relaxation, etc. The simulation is carried out for a large sample of molecules for many time units. We have shown previously[14] that the equilibrium sample contains a Boltzmann distribution of h and c states. Therefore, the end point of any kinetics simulation can be used as a starting sample for a kinetics simulation to a new equilibrium end point.

For chain lengths less then 100 and $v = 0.01$, the helix–coil transition is known to be in the one helix region[6] which means that the probability of formation of two α-helical sequences in one chain is taken to be zero. In fact, the probability of any three event transitions, i.e., some combination of breaking three hydrogen bonds and creating new h states, is extremely small. For example, the probability per unit time of adding three h states to the end of an α-helical sequence is $<10^{-5}$. We neglect all three event transitions with the exception of helix nucleation which is obviously necessary in our model. In each fundamental time unit of duration p^{-1}, a new configuration is selected for each molecule in the sample based on the weighting scheme discussed previously. The actual selection of the new state is made by a random number generator. For example, the molecule chhhhhhhc can make the transition to all of the new states shown in Table I. Also shown in Table I are the probabilities of transition to each possible new state. The largest transition probability is for the molecule to make no transition, i.e., to maintain the original configuration. The probability of a molecule making no transition depends on the configuration of the molecule and on the equilibrium parameters v and w but is usually about 0.97. Transitions in-

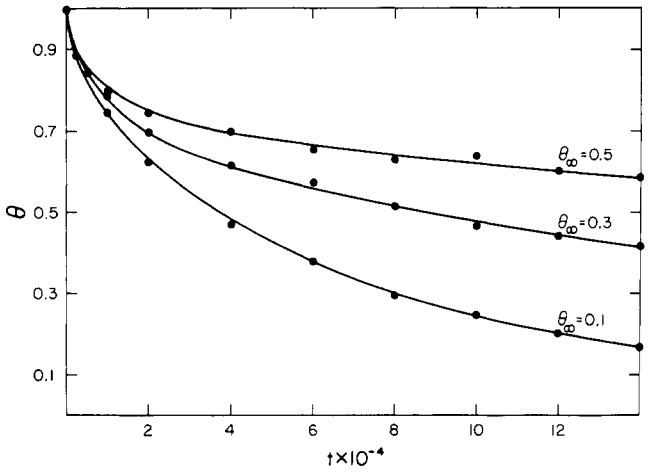

Figure 1. Plots of the fractional hydrogen bonding parameter θ vs. t (in fundamental time units) at chain length 85, for $v = 0.01$. The closed circles (●) represent kinetics data generated using the Monte Carlo kinetics simulation method. Each data point represents an average value using a chain sample of 500 molecules. The solid lines represent the chemical relaxations predicted by the appropriate data in Table IV.

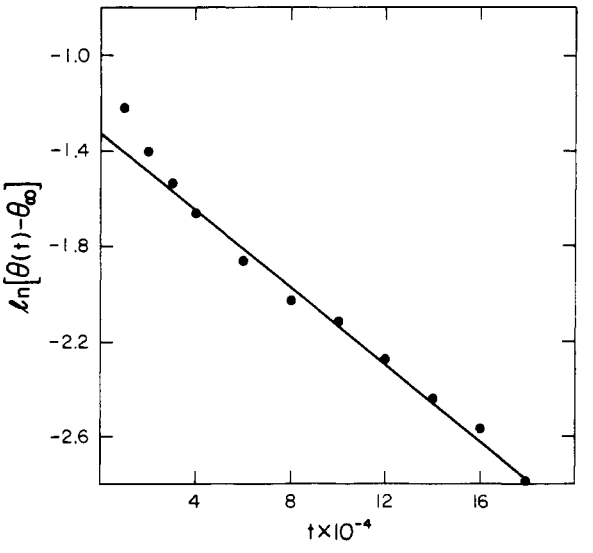

Figure 2. Plot of ln $[\theta(t) - \theta_\infty]$ vs. t (where t is in fundamental time units) at chain length 85 and $v = 0.01$ with $\theta_0 = 1$ and $\theta_\infty = 0.5$. The solid circles (●) represent kinetics data generated using the Monte Carlo kinetics simulation method. Each data point represents an average value using a chain sample of 500 molecules. The solid line represents the slope of the linear portion of the curve obtained by least-squares analysis.

Table I
List of New Configurations with Corresponding Probabilities of Transition for Chain Length 10 and Configuration chhhhhhhc

New configuration	Probability of transition
chhhhhhhhc	$(1-q)^2(1-2\alpha+\alpha^2)$
hhhhhhhhhc	$q(1-q)(1-2\alpha+\alpha^2)$
chhhhhhhhh	$q(1-q)(1-2\alpha+\alpha^2)$
cchhhhhhhc	$\alpha(1-q)(1-2\alpha+\alpha^2)$
chhhhhhhcc	$\alpha(1-q)(1-2\alpha+\alpha^2)$
hhhhhhhhhh	$q^2(1-2\alpha+\alpha^2)$
cchhhhhhhh	$q\alpha(1-2\alpha+\alpha^2)$
hhhhhhhhcc	$q\alpha(1-2\alpha+\alpha^2)$
cchhhhhhcc	$\alpha^2(1-2\alpha+\alpha^2)$
ccchhhhhhc	$\alpha^2(1-q)(1-2\alpha+\alpha^2)$
chhhhhhccc	$\alpha^2(1-q)(1-2\alpha+\alpha^2)$

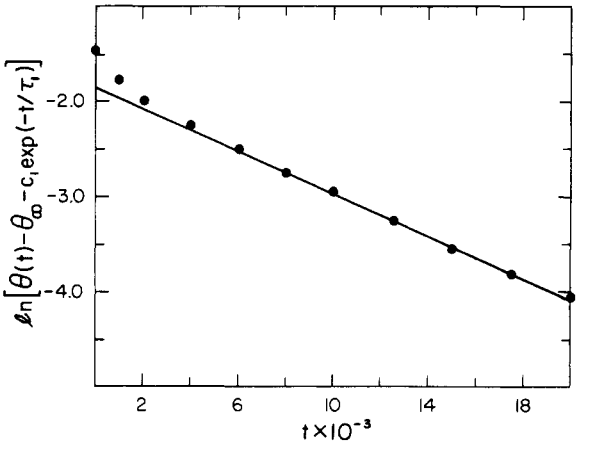

Figure 3. Plot of ln $[\theta(t) - \theta_\infty - c_1 \exp(-t/\tau_1)]$ vs. t (where τ_1 and t are in fundamental time units) at chain length 85 and $v = 0.01$ with $\theta_0 = 1$ and $\theta_\infty = 0.5$. The solid circles (●) represent kinetics data generated using the Monte Carlo kinetics simulation method. Each data point represents an average value using a chain sample of 500 molecules. The solid line represents the slope of the linear portion of the curve obtained by least-squares analysis.

volving formation of an isolated h state are not allowed since the probabilities of these transitions involve powers of the term $(p - 1) = 0$ with $p = 1$. An example of such a forbidden transition is cchhhhhcc → cchhhchcc with transition probability of $\alpha^2 p(1 - \alpha p^3)(1 - q)^4(1 - p)$. Thus our model includes all chemically significant transitions and all end effects for the one helix model of the helix–coil transition.

The chain lengths studied in this paper are 15, 34, and 85 and $v = 0.01$ in all calculations. Starting points $\theta_0 = 1$ and 0 will be used for all chain lengths with simulations carried out to a variety of end points. The objective of this effort is to evaluate the chemically significant part of eq 6 as a function of helix content. Examples of relaxation simulations are shown in Figure 1 for chain length 85 and starting point $\theta_0 = 1$. The usual spectrum[18] of relaxation times in eq 6 is $1/\tau_0 = 0$, $1/\tau_2 > 1/\tau_1$, $1/\tau_3 > 1/\tau_2, \ldots$. All normal modes of relaxation will have decayed out after a time which is long compared with $((1/\tau_2) - (1/\tau_1))^{-1}$ except that associated with $1/\tau_1$. For the remaining portion of the chemical relaxation, $\theta(t)$ approaches θ_∞ at a rate which is proportional to its displacement from equilibrium. Thus τ_1 and c_1 may be determined in this first-order reaction region by using eq 8.

$$\ln [\theta(t) - \theta_\infty] \simeq \ln c_1 - t/\tau_1 \qquad (8)$$

An example of a determination of τ_1 and c_1 is shown in Figure 2 for chain length 85 with $\theta_0 = 1$ and $\theta_\infty = 0.5$. It can be seen that the plot shown in Figure 2 is characterized by nonlinearity during the early time period followed by a substantial time period of linear behavior. c_1 is calculated from the intercept on the ln $[\theta(t) - \theta_\infty]$ axis. After c_1 and τ_1 are calculated, c_2 and τ_2 may be determined using eq 9.

$$\ln [\theta(t) - \theta_\infty - c_1 \exp(-t/\tau_1)] \simeq \ln c_2 - t/\tau_2 \qquad (9)$$

An example of a determination of c_2 and τ_2 is shown in Figure 3 for chain length 85 with $\theta_0 = 1$ and $\theta_\infty = 0.5$. As can be seen in the figure, the early part of the relaxation is nonlinear. The linear portion of the relaxation is of much shorter duration than was the case for the evaluation of c_1 and τ_1. τ_2 is calcu-

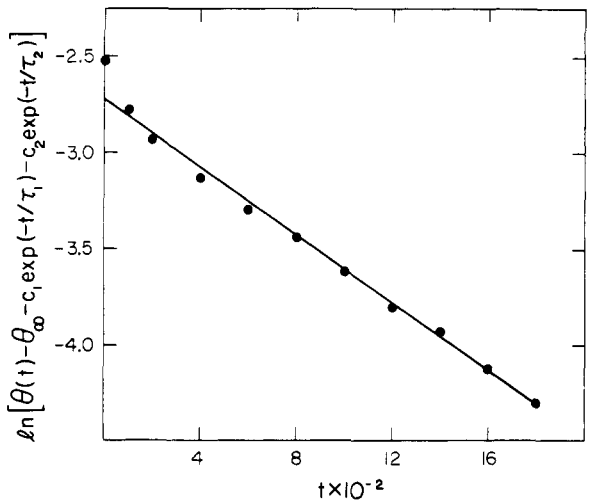

Figure 4. Plot of ln $[\theta(t) - \theta_\infty - c_1 \exp(-t/\tau_1) - c_2 \exp(-t/\tau_2)]$ vs. t (where τ_1, τ_2, and t are in fundamental time units) at chain length 85 and $v = 0.01$ with $\theta_0 = 1$ and $\theta_\infty = 0.5$. The solid circles (●) represent kinetics data generated using the Monte Carlo kinetics simulation method. Each data point represents an average value using a chain sample of 500 molecules. The solid line represents the slope of the linear portion of the curve obtained by least-squares analysis.

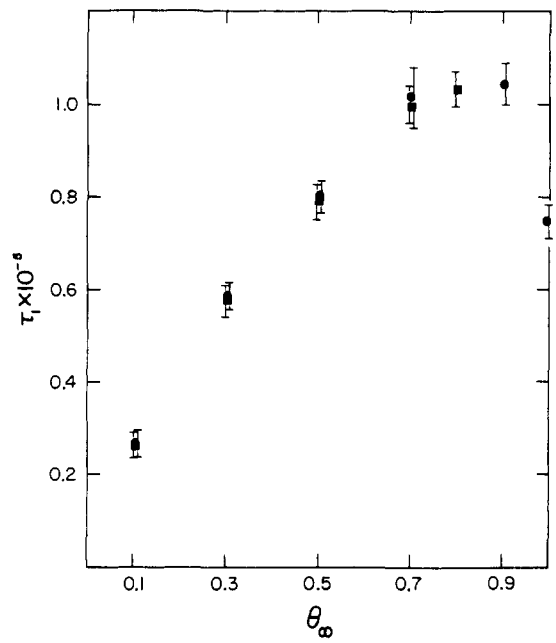

Figure 5. Plots of τ_1 (in fundamental time units) vs. θ_∞ for chain length 15 and $v = 0.01$. The solid circles (●) represent $\theta_0 = 0$, and the solid squares (■) represent $\theta_0 = 1$. The error bars on each data point represent 90% confidence limits.

lated from the slope of the linear portion of the curve and c_2 is calculated from the intercept on the ln $[\theta(t) - \theta_\infty - c_1 \exp(-t/\tau_1)]$ axis. After c_1, τ_1, c_2, and τ_2 have been determined, c_3 and τ_3 may be calculated using eq 10.

$$\ln [\theta(t) - \theta_\infty - c_1 \exp(-t/\tau_1) - c_2 \exp(-t/\tau_2)] \simeq \ln c_3 - t/\tau_3 \quad (10)$$

An example of a determination of c_3 and τ_3 is shown in Figure 4 for chain length 85 with $\theta_0 = 1$ and $\theta_\infty = 0.5$. Note that during the early part of the relaxation there is still some nonlinear behavior. As before, the relaxation time τ_3 and the constant c_3 are calculated from the slope and the intercept, respectively. This method of data analysis is used to determine the chemically significant terms in eq 6 for all relaxations investigated in this paper.

The random number generator used in this work was the generalized Feedback Shift Register Pseudorandon Number Algorithm (GSFR).[20] The primitive trinomial $x^{98} + x^{27} + 1$ was used with a 22 bit word size. All calculations presented in this paper were performed on a PDP8 computer (Digital Equipment Corporation) equipped with 32K of core and Floating Point Processor.

III. Results and Discussion

Shown in Figure 5 is the plot of τ_1 vs. θ_∞ for chain length 15. The starting points for the relaxations are $\theta_0 = 1$ and 0. Ten experiments were run for each starting point and the τ_1's shown in the figure represent the average value and the 90% confidence limit. As can be seen in the figure, for the two starting points proceeding to the same end point, the τ_1's agree within the 90% confidence limit except for $\theta_\infty = 0.9$. The maximum value of τ_1, denoted $\tau_{1,\max}$, occurs near $\theta_\infty = 0.9$ for this very short chain length. For $\theta_0 = 0$, the value of τ_1 increases for increasing θ_∞, reaching a maximum near $\theta_\infty = 0.9$, and then decreases for $\theta_\infty = 1$. For $\theta_0 = 1$ the value of τ_1 increases for increasing θ_∞ reaching a maximum near $\theta_\infty = 0.8$ and then disappears for $\theta_\infty = 0.9$. Since all of the other τ_1's agree quite well as predicted by theory, we interpret the absence of τ_1 at $\theta_\infty = 0.9$ for the starting point $\theta_0 = 1$ to mean that the amplitude associated with the first normal mode of relaxation is very small. It will be seen that this behavior is a general phenomenon for all chain lengths studied. In Figure 6 is shown the plot of τ_1 vs. θ_∞ for chain length 34. As before, the starting points for the relaxations are $\theta_0 = 1$ and 0 with relaxations to the end points indicated in the figure. For the end point $\theta_\infty = 0.9$, the starting points are $\theta_0 = 0$ and 0.5247. As can be seen in the figure, τ_1 shows good agreement within the 90% confidence limit at each end point for both of the starting points with $\tau_{1,\max}$ near $\theta_\infty = 0.5$. For the starting point $\theta_0 = 0$, τ_1 increases with increasing θ_∞ reaching a maximum near $\theta_\infty = 0.5$ and then decreases. For $\theta_0 = 1$, τ_1 increases with increasing θ_∞, reaching a maximum near $\theta_\infty = 0.5$, and then decreases for $\theta_\infty = 0.7$ but is absent for $\theta_\infty = 0.9$. For $\theta_\infty = 0.9$, an additional starting point of $\theta_0 = 0.5247$ was used to verify τ_1 at this end point. As can be seen in the figure, the values of τ_1 at $\theta_\infty = 0.9$ for the starting points $\theta_0 = 0$ and 0.5247 agree within the 90% confidence limits as predicted by theory. In Figure 7 is shown the plot of τ_1 vs. θ_∞ for chain length 85. Again the starting points are $\theta_0 = 1$ and 0 with relaxations to the end points indicated in the figure. For $\theta_\infty = 0.7$, the starting points are $\theta_0 = 0.5$. As before τ_1 shows good agreement within the 90% confidence limits at each end point for both of the starting points with $\tau_{1,\max}$ near $\theta_\infty = 0.5$. For $\theta_0 = 0$, τ_1 increases for increasing θ_∞ reaching a maximum near $\theta_\infty = 0.5$ and then decreases. For the starting point $\theta_0 = 1$, τ_1 increases for increasing θ_∞. At $\theta_\infty = 0.7$, it was not possible to calculate τ_1 because of the small value of c_1 and the scatter of the data. We used an additional starting point of $\theta_0 = 0.5$ to verify τ_1 for $\theta_\infty = 0.7$. As can be seen in the figure, for the two starting points $\theta_0 = 0$ and 0.5, τ_1 agrees within the 90% confidence limits for $\theta_\infty = 0.7$. For $\theta_0 = 1$ and $\theta_\infty = 0.9$, τ_1 was again absent. For chain length 15, $\tau_{1,\max}$ is found at a large value of θ_∞ and the behavior of τ_1 vs. θ_∞ is markedly unsymmetrical. For chain length 34, $\tau_{1,\max}$ has shifted toward $\theta_\infty = 0.5$ and the behavior of τ_1 as a function of θ_∞ has become more symmetrical. For chain length 85, $\tau_{1,\max}$ is near $\theta_\infty = 0.5$ and the behavior of τ_1 as a function θ_∞ has become substantially more symmetrical with the values of τ_1 for $\theta_\infty = 0.1$ and 0.9 equal within the 90% confidence limits. Thus for increasing chain length, τ_1 as a function of θ_∞ appears to be approaching a symmetrical behavior with $\tau_{1,\max}$

Table II
Relaxation Spectra for Chain Length 15 and $v = 0.01$[a]

θ_∞	c_1	$\tau_1 \times 10^{-5}$	c_2	$\tau_2 \times 10^{-3}$	c_3	$\tau_3 \times 10^{-2}$
			$\theta_0 = 1$			
0.1	0.66 ± 0.038	0.27 ± 0.027	0.20 ± 0.014	0.52 ± 0.033		
0.3	0.52 ± 0.02	0.58 ± 0.035	0.17 ± 0.051	0.40 ± 0.031		
0.5	0.34 ± 0.035	0.79 ± 0.042	0.131 ± 0.005	0.34 ± 0.022		
0.7	0.16 ± 0.01	1.0 ± 0.046	0.11 ± 0.017	0.38 ± 0.026		
0.8	0.072 ± 0.005	1.04 ± 0.04				
0.9			0.083 ± 0.005	0.31 ± 0.028	0.02 ± 0.01	0.33 ± 0.071
			$\theta_0 = 0$			
0.1	−0.10 ± 0.01	0.27 ± 0.029				
0.3	−0.31 ± 0.014	0.58 ± 0.031				
0.5	−0.51 ± 0.016	0.80 ± 0.037				
0.7	−0.71 ± 0.022	1.02 ± 0.065				
0.9	−0.90 ± 0.023	1.04 ± 0.052				
0.99	−1.0 ± 0.033	0.75 ± 0.037				
			$\theta_0 = 0.5$			
0.1	0.37 ± 0.044	0.26 ± 0.043				
0.9	−0.36 ± 0.047	1.05 ± 0.053	−0.04 ± 0.026	0.37 ± 0.062		

[a] Experimental errors are 90% confidence limits and values of τ_i are expressed in fundamental time units.

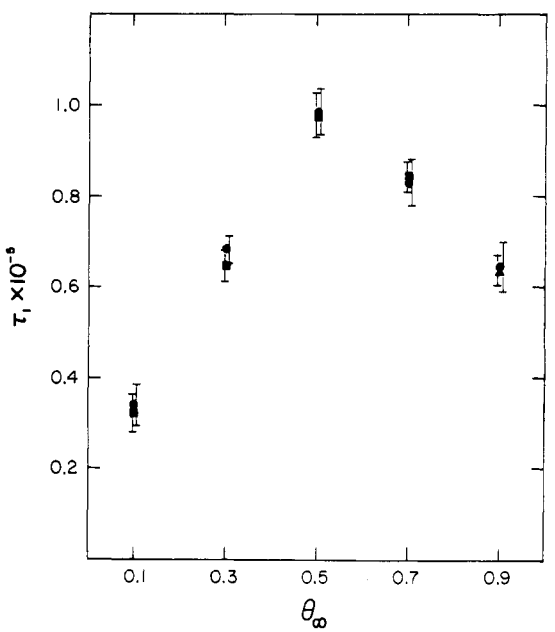

Figure 6. Plots of τ_1 (in fundamental time units) vs. θ_∞ for chain length 34 and $v = 0.01$. The solid circles (●) represent $\theta_0 = 0$, the solid squares (■) represent $\theta_0 = 1$, and the solid triangle (▲) represents $\theta_0 = 0.5247$. The error bars on each data point represent 90% confidence limits.

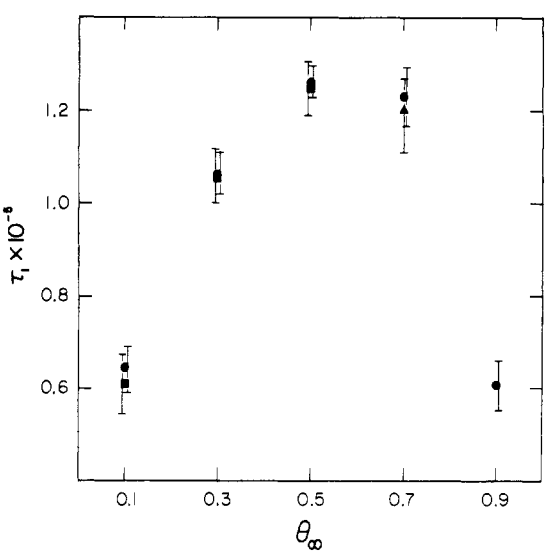

Figure 7. Plots of τ_1 (in fundamental time units) vs. θ_∞ for chain length 85 and $v = 0.01$. The solid circles (●) represent $\theta_0 = 0$, the solid squares (■) represent $\theta_0 = 1$, and the solid triangle (▲) represents $\theta_0 = 0.5$. The error bars on each data point represent 90% confidence limits.

approaching $\theta_\infty = 0.5$. For all three chain lengths τ_1 is missing, i.e., $c_1 \simeq 0$, for the relaxation $\theta_0 = 1 \rightarrow \theta_\infty = 0.9$.

In Tables II, III, and IV are shown the chemically significant terms of eq 6 for all of the relaxations studied. For the starting point $\theta_0 = 0$, the relaxations are described well with only one exponential term. The data for chain length 15, shown in Table II, indicate that for all end points the reaction can be described by the eq $\theta(t) = \theta_\infty + c_1 \exp(-t/\tau_1)$, all other c_i's being $\simeq 0$. For chain length 34 and $\theta_0 = 0$, shown in Table III, two exponential terms are needed for $\theta_\infty = 0.7$ and 0.9. However, as can be seen, the constant weighting of the second-exponential term is small in each case.

For chain length 85 and $\theta_0 = 0$, shown in Table IV, two exponential terms are needed for all end points except $\theta_\infty = 0.1$. However, as before, the c_i's weighting the second exponential term are all small and $c_i \simeq 0$ for $i > 2$. Comparing the data for all three chain lengths with $\theta_0 = 0$, it can be seen that the c_1 corresponding to each end point is the same at all three chain lengths within the 90% confidence limits indicated in the table except for the relaxation $\theta_0 = 0 \rightarrow \theta_\infty = 0.9$ at chain length 85. This is an obvious result since with c_2 small and all other c_i's $\simeq 0$, $\theta_\infty + \Sigma_i c_i \equiv 0$ at $t = 0$ from eq 6.

For $\theta_0 = 1$, a more complicated relaxation spectrum is produced resulting from fast initial reactions. The data for chain length 15, shown in Table II, indicate that two exponential terms are sufficient to accurately describe the relaxations with all other c_i's $\simeq 0$. For $\theta_\infty = 0.1$, 0.3, 0.5, and 0.7, τ_1 and τ_2 are separated by approximately two orders of magnitude indicating that the initial fast reaction is very short in duration. For $\theta_\infty = 0.9$, the first relaxation time shown in the table is of

Table III
Relaxation Spectra for Chain Length 34 and $v = 0.01$[a]

θ_∞	c_1	$\tau_1 \times 10^{-5}$	c_2	$\tau_2 \times 10^{-4}$	c_3	$\tau_3 \times 10^{-3}$	c_4	$\tau_4 \times 10^{-2}$
				$\theta_0 = 1$				
0.1	0.66 ± 0.039	0.32 ± 0.042	0.17 ± 0.012	0.19 ± 0.025	0.062 ± 0.003	0.29 ± 0.027		
0.3	0.45 ± 0.02	0.65 ± 0.037	0.17 ± 0.025	0.24 ± 0.049	0.064 ± 0.006	0.30 ± 0.036		
0.5	0.27 ± 0.02	0.98 ± 0.05	0.16 ± 0.022	0.25 ± 0.064	0.06 ± 0.014	.29 ± 0.054		
0.7	0.10 ± 0.025	0.85 ± 0.034	0.12 ± 0.025	0.27 ± 0.064	0.08 ± 0.02	0.32 ± 0.061		
0.9					0.074 ± 0.005	0.73 ± 0.06	0.026 ± 0.002	0.93 ± 0.08
				$\theta_0 = 0$				
0.1	−0.102 ± 0.005	0.34 ± 0.045						
0.3	−0.31 ± 0.011	0.69 ± 0.028						
0.5	−0.50 ± 0.034	0.99 ± 0.05						
0.7	−0.72 ± 0.014	0.83 ± 0.053	0.025 ± 0.003	0.3 ± 0.11				
0.9	−0.93 ± 0.026	0.65 ± 0.056	0.032 ± 0.002	0.29 ± 0.063				
				$\theta_0 = 0.5247$				
0.9	−0.27 ± 0.05	0.64 ± 0.033	−0.08 ± 0.05	0.27 ± 0.064	−0.04 ± 0.046	0.72 ± 0.04		

[a] Experimental errors are 90% confidence limits and values of τ_i are expressed in fundamental time units.

the same order of magnitude as τ_2 for all other end points at this chain length. We assume $c_1 \simeq 0$ and associate the first constant and first relaxation time calculated with c_2 and τ_2, respectively. As a check, we used the starting point $\theta_0 = 0.5$ with $\theta_\infty = 0.9$ and calculated c_1, τ_1, c_2, and τ_2 for this relaxation. The results shown in Table II indicate that our assumption was correct since τ_2 agrees for both starting points within the 90% confidence limits. For chain length 34 shown in Table III, four exponential terms are needed to describe the relaxations with τ_1, τ_2, τ_3, and τ_4 separated by about one order of magnitude. For $\theta_\infty = 0.9$ the first calculated relaxation time is of the same order of magnitude as τ_3 for all other end points at this chain length. We assigned the first calculated constant and relaxation time to c_3 and τ_3, respectively, and the second calculated constant and relaxation time to c_4 and τ_4, respectively. These assumptions were verified by using the starting point $\theta_0 = 0.5247$ with $\theta_\infty = 0.9$. From this relaxation we calculated three constants and three corresponding relaxation times which are shown in Table III. As can be seen, τ_1 and τ_2 for $\theta_0 = 0$ and 0.5247 agree within the 90% confidence limits, while τ_3 for $\theta_0 = 1$ and 0.5247 also agree within the 90% confidence limits. This experiment verifies our assumption about the assignment of the constants and relaxation times for the relaxation $\theta_0 = 1 \rightarrow \theta_\infty = 0.9$. The data for chain length 85, shown in Table IV, indicate that the relaxations are described well by three exponential terms with τ_1, τ_2, and τ_3 separated by about one order of magnitude. For the relaxation $\theta_0 = 1 \rightarrow \theta_\infty = 0.7$, it was not possible to calculate c_1 and τ_1 using the standard method described previously because of the scatter in our data. We used starting points $\theta_0 = 0.24$ and 0.5 to verify the value of τ_1 and τ_2 at $\theta_\infty = 0.7$. We then assumed a value of $c_1 = 0.08$ and the known value of τ_1 for the relaxation $\theta_0 = 1 \rightarrow \theta_\infty = 0.7$ to obtain a value of τ_2 which agreed with τ_2 obtained using the other starting points. For $\theta_\infty = 0.9$, we again assumed $c_1 = 0$. As can be seen, τ_2 at this end point agrees with the value of τ_2 obtained using $\theta_0 = 0$. In Figure 1 are shown several examples of Monte Carlo kinetics experiments for chain length 85. The experiments shown in the figure are for $\theta_0 = 1$ relaxing to the indicated end points. The solid curves show the relaxations predicted by using the appropriate data in Table IV. As can be seen from the results in this figure, the method of data analysis presented in this paper gives results which are consistent with the Monte Carlo data. Similar consistency was found for the other relaxation data presented in Tables II, III, and IV when compared to the Monte Carlo kinetics experiments. For all three chain lengths studied, it

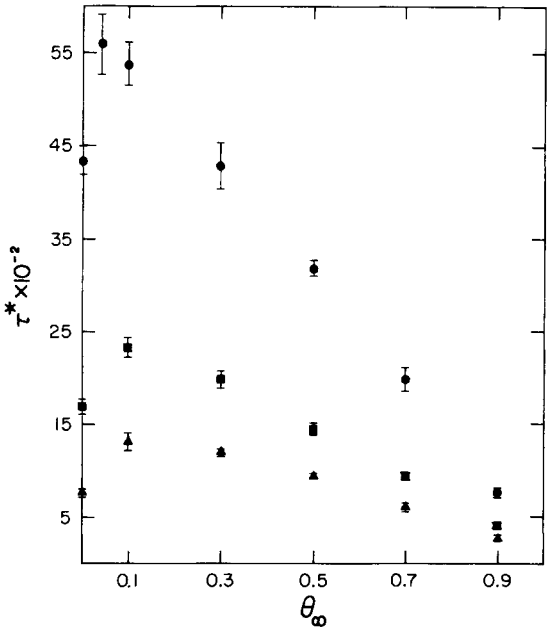

Figure 8. Plots of τ^* (in fundamental time units) vs. θ_0. The solid circles (●) represent data for chain length 85, the solid squares (■) represent data for chain length 34, and the solid triangles (▲) represent data for chain length 15. The error bars on each data point represent 90% confidence limits.

was found that the τ_i's were a function only of θ_∞, while the c_i's were a function of both θ_0 and θ_∞, in agreement with the results of Chay and Stevens[23] who used a zipper model of the kinetics of the helix–coil transition.

In Figure 8 are shown the mean relaxation times τ^* as a function of θ_∞ for chain lengths 15, 34, and 85. τ^* was calculated using the familiar expressions $1/\tau^* = [1/(\theta_0 - \theta_\infty)][d\theta/dt]_{t=0}$. The starting point for all of the relaxations shown in the figure is $\theta_0 = 1$. As can be seen τ^* reaches a maximum at a very small value of θ_∞ for all three chain lengths. It has been proposed theoretically[5] and demonstrated experimentally that for $N \rightarrow \infty$ τ^* obeys eq 11.

$$\tau^* = \{k_f[(w - 1)^2 + 4v^2]\}^{-1} \quad (11)$$

Thus τ^* is symmetrical around the maximum value of τ^* which occurs when $w = 1$. For $w = 1$, we calculated[4] $\theta_\infty = 0.064$,

Table IV
Relaxation Spectra for Chain Length 85 and $v = 0.01$[a]

θ_∞	c_1	$\tau_1 \times 10^{-5}$	c_2	$\tau_2 \times 10^{-4}$	c_3	$\tau_3 \times 10^{-3}$
			$\theta_0 = 1$			
0.1	0.74 ± 0.037	0.61 ± 0.069	0.11 ± 0.013	0.46 ± 0.068		
0.3	0.46 ± 0.044	1.06 ± 0.068	0.198 ± 0.008	0.8 ± 0.12	0.043 ± 0.002	0.45 ± 0.05
0.5	0.27 ± 0.025	1.25 ± 0.06	0.15 ± 0.027	1.04 ± 0.022	0.065 ± 0.003	1.6 ± 0.22
0.7	0.08	1.23	0.13 ± 0.058	1.49 ± 0.062	0.07 ± 0.012	1.97 ± 0.061
0.9			0.059 ± 0.008	0.42 ± 0.06	0.035 ± 0.003	0.56 ± 0.095
			$\theta_0 = 0$			
0.1	−0.098 ± 0.004	0.645 ± 0.052				
0.3	−0.31 ± 0.014	1.07 ± 0.045	0.011 ± 0.001	0.9 ± 0.7		
0.5	−0.53 ± 0.012	1.26 ± 0.033	0.029 ± 0.001	1.3 ± 0.26		
0.7	−0.74 ± 0.016	1.23 ± 0.063	0.06 ± 0.011	1.3 ± 0.48		
0.9	−0.99 ± 0.011	0.61 ± 0.055	0.11 ± 0.013	0.47 ± 0.94		
			$\theta_0 = 0.5$			
0.7	−0.14 ± 0.019	1.2 ± 0.08	−0.05 ± 0.012	1.2 ± 0.49		
			$\theta_0 = 0.24$			
0.7	−0.43 ± 0.026	1.2 ± 0.13	−0.03 ± 0.012	1.5 ± 0.45		

[a] Experimental errors are 90% confidence limits and values of τ_i are expressed in fundamental time units.

0.015, and 0.003 for chain lengths 85, 34, and 15, respectively. We cannot verify the location of τ^*_{max} at these low values of θ_∞ using our model because of the experimental uncertainties indicated in the figure. However, the results shown in Figure 8 appear to be consistent with the theoretically predicted results even though eq 11 is rigorously valid only for $N \to \infty$. Comparing the mean relaxation times in Figure 8 with the values of τ_1 shown in Figures 5, 6, and 7, it can be seen that τ_1 is always larger than τ^* by at least one order of magnitude. τ^* is a readily accessible experimental quantity and is usually considered to be a measure of the time required by the kinetic process. Unfortunately τ^* apparently does not reflect the correct order of magnitude of the slowest relaxation process. A brief examination of the data in Tables II, III, and IV will show why this is the case. For chain length 34 for the relaxation $\theta_0 = 1 \to \theta_\infty = 0.7$, $\tau^* = [\Sigma c_i/\tau_i]^{-1} = 3383$ which does not agree with the value shown in Figure 8. If we assume that $c_4 = 0.02$ and $\tau_4 = 0.2 \times 10^2$, which means that there is an additional very fast initial reaction which we are unable to measure because of the scatter in the Monte Carlo data, then $\tau^* = 772$ which is near the value given in Figure 8. This means that a relaxation time with its characteristic amplitude which has a negligible effect on the time course of the chemical relaxation has a disproportionately large influence on the mean relaxation time τ^*.

In Figure 9 is shown a plot of τ^* as a function of chain length. τ^* exhibits an increasing linear behavior as a function of chain length for all values of θ_∞ shown in the figure. This is not a surprising result since these chain lengths are all in the one helix region. Similar results were obtained by Nagayama and Wada[12] using NMR spectroscopy on poly(γ-benzl L-glutamate) for chain lengths 35, 85, and 250, and $v \simeq 0.01$. These authors reported a relaxation time associated with the helix–coil transition of 7×10^{-4} s at $\theta_\infty = 0.55$ for chain length 85 and a value of 1.1×10^{-3} s at $\theta_\infty = 0.55$ for chain length 250. These values seem quite slow and in fact Tsuji et al.[21] have recently reported a value for τ^* of 3×10^{-6} for poly(α-L-glutamic acid) at chain length 250 and $v \simeq 0.055$. This value of τ^* is of the order of magnitude usually associated with long chain lengths. It is unknown what effect the difference in polymer or value of v might have on τ^* although such a large value of v shifts the validity of the one-helix model to chain lengths less than 20.

For the purpose of the discussion to follow, we will assume

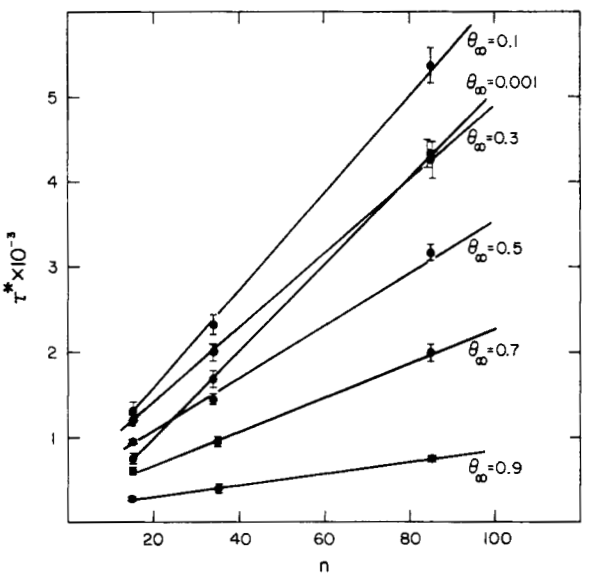

Figure 9. Plots of τ^* (in fundamental time units) vs. chain length for $\theta_\infty = 0.003, 0.1, 0.3, 0.5, 0.7$, and 0.9. The error bars on each data point represent 90% confidence limits. The solid lines are constructed through the data points at each value of θ_∞.

that the value of τ^* for chain length 85 reported by Nagayama and Wada is at least an upper bound of the correct value. For chain length 85, $v = 0.01$, and $\theta_\infty = 0.55$ the value of w is calculated to be 1.077 and from eq 11 k_f is calculated to be 2.3×10^5 s^{-1}. From this value of k_f, we calculated a value of $p = 2.3 \times 10^7$ s^{-1} and therefore our fundamental time unit $p^{-1} = 4 \times 10^{-8}$ s. For the relaxation $\theta_0 = 1 \to \theta_\infty = 0.5$ at chain length 85, τ_1, τ_2, and τ_3 are $1.25 \times 10^5 p^{-1}$, $1.04 \times 10^4 p^{-1}$, and $1.6 \times 10^3 p^{-1}$, respectively, and therefore $\tau_1 = 5 \times 10^{-3}$ s, $\tau_2 = 4.2 \times 10^{-4}$ s, and $\tau_3 = 6.4 \times 10^{-5}$ s. The third exponential term for this reaction will contribute less than 0.01 to eq 6 after 1.2×10^{-4} s, the second exponential term for this reaction will contribute less than 0.01 to eq 6 after 1.1×10^{-3} s, and the first exponential term will contribute less than 0.01 to eq 6 after 1.6×10^{-2} s. Therefore this reaction is first order after only 7% of the relaxation has occurred. In addition, 1.6×10^{-2} s seems a long time for the reaction and therefore 4×10^{-8} s must surely be an upper bound for p^{-1}.

Using NMR spectroscopy, Ferretti and Paolillo[9] and Ferretti and Ninham[10] have reported a relaxation time associated with the helix–coil transition of $\tau \geq 10^{-1}$ s. These authors have attributed this slow relaxation time to long lived pure random coil chains in the sample. This interpretation means that a significant concentration of pure random coil chains must survive as pure random coils for at least 10^{-1} s. A second interpretation[11,12] has suggested that doublet peaks in the NMR spectra are caused by polydisperse samples. We resolve the apparent conflict using our Monte Carlo kinetics simulation. At chain length 85, we used one molecule which we allowed to make normal transitions. When the molecule contained a helix segment, the helical segment would grow and shrink according to the probability scheme discussed previously. Occasionally the molecule would make the transition to the pure random coil. When this occurred we counted the number of fundamental time units which passed before the molecule nucleated. Averaged over 2×10^8 time units, the equilibrium value of θ was 0.5 and the molecule made the transition to the pure random coil 3818 times. The average lifetime of the pure random coil was 12 260 fundamental time units. Using the value of p^{-1} calculated previously, the pure random coil survived for 5×10^{-4} s on the average. The longest time period that any random coil survived was 4.3×10^{-3} s. Since the value of p^{-1} used is considered to be an upper bound of the correct value, our estimate of the survival time of the pure random coil must also be considered an upper bound. These calculations show that the pure random coil does not survive long enough to be measured by NMR spectroscopy. Therefore according to the stochastic model of the kinetics of the helix–coil transition the doublet peaks which appear in NMR spectra do not represent long lived helix and random coil species.

Acknowledgment. This work was supported by a grant (GB-39851) from the National Science Foundation. One of us (R.A.S.) is also a United States Public Health Service Career Development Awardee (GM-38-7516).

References and Notes

(1) M. V. Volkenstein, "Configurational Statistics of Polymer Chains", Interscience, New York, N.Y., 1963.
(2) T. M. Birshtein and O. B. Ptitsyn, "Conformations of Macromolecules", Interscience, New York, N.Y., 1966.
(3) P. J. Flory, "Statistical Mechanics of Chain Molecules", Interscience, New York, N.Y., 1969.
(4) D. Poland and H. A. Scheraga, "Theory of the Helix-Coil Transitions in Biopolymers", Academic Press, New York, N.Y., 1970.
(5) G. Schwarz, *Biopolymers*, **6**, 873 (1968).
(6) R. L. Jernigan and J. A. Ferretti, *J. Chem. Phys.*, **62**, 2519 (1975).
(7) D. Poland and H. A. Scheraga, *J. Chem. Phys.*, **45**, 2071 (1966).
(8) D. A. McQuarrie, J. P. McTague, and H. Reiss, *Biopolymers*, **3**, 657 (1965).
(9) J. A. Ferretti and L. Paolillo, *Biopolymers*, **7**, 155 (1969).
(10) J. A. Ferretti and B. W. Ninham, *Macromolecules*, **3**, 30 (1970).
(11) R. Ullman, *Biopolymers*, **9**, 491 (1970).
(12) K. Nagayama and A. Wada, *Biopolymers*, **14**, 2489 (1975).
(13) S. Lifson and A. Roig, *J. Chem. Phys.*, **34**, 1963 (1961).
(14) D. E. Neves and R. A. Scott III, *Macromolecules*, **9**, 554 (1976).
(15) R. A. Scott III, unpublished results.
(16) T. R. Chay and C. L. Stevens, *Macromolecules*, **8**, 531 (1975).
(17) J. A. Ferretti, B. W. Ninham, and V. A. Parsegian, *Macromolecules*, **3**, 34 (1970).
(18) B. Widom, *Science*, **148**, 1555 (1965).
(19) G. Schwarz and J. Seelig, *Biopolymers*, **6**, 1263 (1968).
(20) T. G. Lewis and W. H. Payne, *J. ACM*, **20**, 3, 456 (1973).
(21) Y. Tsuji, T. Yasunaga, T. Sano, and H. Ushio, *J. Am. Chem. Soc.*, **98**, 813 (1976).
(22) E. M. Bradbury, C. Crane-Robinson, and P. G. Hartman, *Polymer*, **14 (11)**, 543 (1973).
(23) T. R. Chay and C. L. Stevens, *Biopolymers*, **12**, 2563 (1973).
(24) G. Schwarz, *Rev. Mod. Phys.*, **40**, 206 (1968).
(25) M. E. Craig and D. M. Crothers, *Biopolymers*, **6**, 385 (1968).

Block Copolypeptides. 1. Synthesis and Solid State Conformational Studies

T. Hayashi, A. G. Walton, and J. M. Anderson*

Department of Macromolecular Science, Case Western Reserve University, Cleveland, Ohio 44106. *Received August 9, 1976*

ABSTRACT: Triblock copolypeptides of γ-benzyl L-glutamate (G) and L-leucine or L-valine of high molecular weight have been prepared. The solubilities and solution conformation were determined and compared with random copolymers of similar composition as well as the appropriate homopolypeptides. Characterization of the secondary structure in the solid state was undertaken as part of an investigation into the solid state properties of this new class of materials. Infrared and solid state measurements indicate that the G and L-leucine blocks assume an α-helical conformation and L-valine blocks a β-sheet structure. Polarized infrared measurements showed the chain axis in oriented films to be parallel to the orientation direction. Further solid state characterization of the tertiary structure and mechanical properties of the block copolypeptides will be reported in succeeding papers.

It is well known that copolymer properties can be profoundly influenced by the presence of blocks, i.e., long sequences of one of the comonomers, especially if these are long and numerous enough to segregate into separate phases of glasslike or crystalline domains. Among copolymers with such long blocks, it is possible to distinguish several types, namely block copolymers made by sequential homopolymerization (for example, A–B–A type triblock copolymers) and statistically random copolymers made by conventional copolymerization with monomer concentrations and reactivity ratios which lead to block structures. Many copolymers are of interest in which the molecules consist of long blocks capable of precipitating in glasslike or crystalline domains separated by amorphous chain segments. The glasslike or crystalline domains form tie points, i.e., quasi-cross-links, which bind the amorphous chains into a network structure similar to that of conventionally cross-linked elastomers. The reversible nature of such tie points bestows upon these materials the special properties which permit their use as thermoplastic elastomers.

Of the synthetic polypeptides which have been used as materials at one time or another (synthetic silk fiber analogues, surface coatings, microphone piezoelectric membranes, biocompatible materials), all have been either derivatives of